Case Studies in Thermal Engineering 82 (2026) 108145

Contents lists available at ScienceDirect

Case Studies in Thermal Engineering

journal homepage: www.elsevier.com/locate/csite

A hybrid finned-PCM and nanoparticle strategy for high-efficiency passive cooling of photovoltaic modules: Experimental study

Menna M. Hamed [a], Mohamed R. Salem [a,b,*], Abdulmajeed D. Aldabesh [b], Sayed A. Abdel-Moneim [a], Ashraf E. Elmohlawy [a]

[a] Mechanical Engineering Department, Faculty of Engineering at Shoubra, Benha University, 108 Shoubra St., 11629, Cairo, Egypt
[b] Department of Mechanical Engineering, Faculty of Engineering, Al-Baha University, 65527, Al-Baha, Saudi Arabia

ARTICLE INFO

Keywords:
Photovoltaic thermal management
Nano-enhanced PCM
Semicircular fin geometry
Passive cooling
Hybrid thermal management

ABSTRACT

The present study investigates a passive cooling strategy for photovoltaic thermal management based on a hybrid system combining phase change material (PCM), alumina nanoparticles, and semicircular rod (SCR) fins. An experimental comparison is conducted between an uncooled reference case, a PCM-only configuration, and finned-PCM systems employing complete circular rod (CCR) and SCR fin geometries over a range of fin pitch ($20\% \leq \lambda \leq 33.3\%$) and spacing ($16\% \leq \delta \leq 48\%$) ratios. The optimal SCR configuration is further examined with alumina nanoparticle loadings between 0.25 and 1.0 wt%. The results indicate that fin integration significantly enhances thermal regulation, with SCR fins providing greater temperature reduction than CCR designs. Under identical operating conditions, the optimal SCR configuration ($\lambda = 20\%$, $\delta = 48\%$) achieves a relative temperature reduction (η) of 62.3% and limits the final surface temperature to 51.0 °C, compared to 89.0 °C for the uncooled case. Incorporating 1.0 wt% alumina nanoparticles further improve performance, yielding a maximum η of 65.9%, a minimum final temperature of 48.8 °C, and an extension of the operating period below 45 °C by 35 min. Although electrical efficiency was not directly measured, the observed reduction in operating temperature, when interpreted using established photovoltaic temperature coefficients, suggests a potential improvement in electrical performance. These findings demonstrate the effectiveness of the hybrid SCR fin and nano-PCM configuration as a fully passive approach for photovoltaic applications.

1. Introduction

Efficient thermal regulation is essential for systems whose performance and reliability are sensitive to temperature fluctuations. With the growing global demand for sustainable energy solutions, advanced thermal management strategies utilizing innovative materials and optimized geometries have attracted significant attention [1–4]. PCM is particularly promising for this role due to its capacity to absorb and release large amounts of latent heat during phase transitions while maintaining a nearly constant temperature, providing effective thermal buffering [5–8]. This unique property makes them ideal for applications in building systems, electronic devices, and renewable energy. In PV systems, which represent the fastest-growing renewable energy source, overheating is a major

* Corresponding author. Mechanical Engineering Department, Faculty of Engineering at Shoubra, Benha University, 108 Shoubra St., 11629, Cairo, Egypt.
E-mail addresses: me_mohamedreda@yahoo.com, mohamed.abdelhamid@feng.bu.edu.eg (M.R. Salem).

https://doi.org/10.1016/j.csite.2026.108145
Received 6 January 2026; Received in revised form 31 March 2026; Accepted 5 May 2026
Available online 6 May 2026
2214-157X/© 2026 The Authors. Published by Elsevier Ltd. This is an open access article under the CC BY license (http://creativecommons.org/licenses/by/4.0/).

limitation. Crystalline silicon modules experience significant efficiency losses when their operating temperature exceeds 25 °C, leading to reduced power output and accelerated degradation [9–12]. While various active and passive cooling strategies exist [13,14], PCM-based regulation offers a compelling passive solution by leveraging this latent heat absorption to directly mitigate temperature rise [13,15], and has consequently seen widespread application in solar energy systems [16–18]. A primary limitation of PCM, however, is its low intrinsic thermal conductivity, which restricts heat diffusion and can limit its effectiveness under high heat fluxes. To address this, fin structures are often incorporated to enhance heat transfer into the PCM bulk. Fins increase the effective surface area for heat exchange, promote faster melting and solidification cycles, and improve overall thermal reliability under dynamic conditions [19,20]. When integrated with PV systems, this finned-PCM configuration creates a synergistic effect, combining high-capacity latent heat storage with enhanced thermal conductivity to improve cooling performance and energy efficiency [21–23].

When integrated into a PV system, an appropriately selected PCM can reduce the module's operating temperature, thereby improving solar-to-electrical conversion efficiency [19,24–28]. Finite volume simulations of PV/PCM systems with various PCM configurations over a 24-h day-night cycle in arid and semi-arid climates showed that optimized designs can lower module temperature by up to 17.5 °C, resulting in a 5.8% increase in annual electricity generation. Biwole et al. investigated the use of PCM attached to the back of solar panels for passive thermal regulation. A validated numerical model demonstrated that a PCM layer can maintain the panel temperature below 40 °C for 80 min under 1000 W/m^2 of solar radiation [29]. This foundational work highlights the potential of PCM but also underscores the limitations imposed by its low thermal conductivity. Soliman et al. investigated PCM integration into a bifacial PV system and reported a reduction in cell temperature of up to 19.8 °C for both top and bottom cells, alongside a power gain of 27.21 W/m^2 and an exergy efficiency increase of 1.09% [30]. The challenge of managing high heat flux under passive operation, however, extends far beyond photovoltaics. Modern high-power electronic components, such as central processing units (CPUs), graphics processing units, and power converters, face a similar and critical need for advanced thermal management solutions. Effective heat dissipation is essential in electronics to maintain processing speeds, prevent performance throttling, and ensure long-term reliability. Passive cooling solutions are highly valued in this domain for their simplicity, zero operational energy cost, and silent operation [31]. In this context, PCM-based heat sinks have shown great promise for electronics, leveraging latent heat absorption to control temperature spikes during periods of high-power demand [32,33]. Therefore, the strategies explored in this study for enhancing PCM performance are directly applicable to the overarching field of thermal management for both energy and electronics systems.

A major limitation of phase change materials is their inherently low thermal conductivity, which restricts heat transfer and reduces performance under dynamic thermal conditions [34,35]. This limitation has motivated the development of hybrid cooling systems that combine PCM with auxiliary materials or geometric modifications to enhance heat transfer. Hybrid cooling approaches integrating active and passive methods, such as PV/T systems combining PCM and water cooling, have demonstrated improved thermal and electrical performance. Reviews by Zheng and Zhou and Emmanuel et al. highlighted that water is an efficient working fluid due to its high heat capacity, availability, and cost-effectiveness, and emphasized the critical influence of absorber design on overall system performance [36,37]. Further experimental studies examined PV/T operation under varying conditions. Abdul et al. reported that increasing water flow beyond 0.082 kg/s did not result in additional PV temperature reduction, with thermal efficiencies ranging from 38.8% to 43.1% [38]. Joo et al. found that a glazed PV/T module with a transparent film achieved a maximum efficiency of 71.1% owing to reduced reflectivity and improved optical transmission [39]. Recent numerical studies continue to quantify these benefits. For instance, Alipour et al. [40] found that integrating metal foam into a PVT/PCM system improved thermal efficiency by 25.4% over a PCM-only system. Similarly, Parach et al. [41] showed that taller fins in a PVT/PCM system significantly reduced PV temperatures, with an optimal electrical efficiency of 13.5% achieved under specific turbulent flow conditions. Further experimental studies examined PV/T operation under varying conditions. Despite these advantages, PV/T systems are characterized by increased structural complexity, higher construction costs, auxiliary energy consumption, and maintenance requirements. Consequently, fully passive PCM-based cooling configurations enhanced through geometric design represent a simpler and more cost-effective alternative, motivating further experimental investigation.

The incorporation of fins into PCM-based systems has been widely adopted as an effective means of enhancing heat dissipation. Semicircular tubular fins provide a favorable curvature geometry that increases heat transfer surface area while maintaining compact dimensions, thereby improving heat exchange with the surrounding PCM [42]. Beyond compensating for the low thermal conductivity of PCM, fin integration offers a practical solution for thermal regulation in confined spaces [43]. Several studies have explored alternative fin geometries to further improve PCM performance. Huang et al. introduced a fractal tree-shaped fin and demonstrated reductions of 34.5% and 49.2% in melting and solidification times, along with improvements of 49.4% and 96.4% in energy storage and discharge rates compared with rectangular fins [44]. Extending this concept, Hosseinzadeh et al. [45] analyzed a triplex-tube PCM heat exchanger enhanced by tree-like fins and hybrid nanoparticles, demonstrating that the combination reduced solidification time by 78% and that tree-like fins alone significantly outperformed rectangular fins. Oliveski et al. analyzed rectangular fins with varying aspect ratios and fin area fractions, showing that increased fin area shortened melting time but reduced energy absorption [46]. Bria et al. investigated PCM thickness in finned PV/PCM systems under the climatic conditions of Oujda, Morocco, identifying 0.06 m as the optimal thickness [47]. Samakoush et al. reported that a triangular fin design increased the PCM melting rate by 57.56% relative to an unfinned cavity [48]. Nature-inspired fin configurations have also been proposed. Li et al. and Jiang et al. designed bifurcated fractal fins modeled after leaf veins and reported improved temperature control compared with rectangular fins in PV/PCM systems [49–51]. Chibani et al. conducted two-dimensional simulations of PV/PCM systems with different fin materials and inclination angles and concluded that these parameters had negligible influence on PCM enthalpy, liquid fraction, or solar cell temperature [52]. Zhang et al. numerically examined the influence of PCM thickness, fin length, arrangement, and number, concluding that fin number had the most pronounced effect on thermal management, while longer fins enhanced heat transfer but reduced temperature uniformity [53].

Furthermore, composites of fins with porous media show great promise, as demonstrated by Mohammadpour et al. [54], who found that copper foam integration in a finned-tube heat exchanger reduced PCM melting time by over 73%. Collectively, these studies demonstrate the importance of fin geometry but largely focus on configurations that represent a trade-off between increased conductive surface area and the ability to organize convective flow. This work identifies a critical gap concerning the application of SCR fins, a geometry that inherently offers both enhanced conductive contact area and a flat-facing surface that can guide buoyancy-driven natural convection within the molten PCM. To the best of the authors' knowledge, a systematic experimental investigation of SCR fins for PV/PCM cooling has not been previously reported.

In addition to geometric enhancement, the integration of nanoparticles into PCM has emerged as a promising approach to overcome low thermal conductivity. Dispersing metallic or metal-oxide nanoparticles within the PCM matrix enhances heat transfer pathways and improves energy storage and release characteristics [55,56]. This nano-engineering strategy directly addresses one of the primary limitations of PCM and broadens its applicability in advanced thermal management systems [57–59]. Several studies have confirmed the effectiveness of nano-enhanced PCM in photovoltaic applications. A hybrid composite of polyethylene glycol 1500 with 3 wt% graphene nanoplatelets and CuO nanoparticles achieved a 91.8% increase in thermal conductivity compared to pure PCM [60]. Abdelrahman et al. demonstrated that Al_2O_3-based nano-PCM combined with cylindrical hollow fins significantly improved PV cooling performance, with outcomes strongly dependent on nanoparticle concentration and fin placement [60]. Zarma et al. reported that incorporating alumina, SiO_2, and CuO nanoparticles reduced PV temperature fluctuations by approximately 12 °C and increased electrical efficiency by 8% [61]. Abdelrazik et al. further reported that graphene nanoplatelet-paraffin composites in a hybrid PV/T system achieved a 22% increase in electrical efficiency at 10 wt% nanoparticle loading relative to conventional PV systems [62]. It is important to note that such enhancements can involve trade-offs; for example, Najafpour et al. [63] reported that the optimal geometry for a nanofluid-cooled heat sink improved thermal efficiency but at the cost of increased pressure drop, lowering the overall performance metric. Lin et al. found that the integration of PCM into an air-based PV/T collector increased system efficiency from 37.6% to 40.2% while boosting latent heat utilization from 13.3% to 79.5% [64]. Nevertheless, these systems remain influenced by auxiliary components and operating conditions.

Previous numerical and experimental studies have demonstrated the efficacy of rectangular [46,48], fractal [44,49], and circular hollow fins [61] in improving PCM performance. While these studies have advanced the understanding of fin-enhanced PCM systems, they have predominantly focused on geometries that represent a fundamental trade-off: maximizing conductive surface area often comes at the expense of impeding natural convection. For instance, dense arrays of rectangular or circular fins can restrict fluid motion, while fractal designs prioritize branching conduction over convective guidance. This creates a clear experimental gap: a lack of systematic investigation into a fin geometry that is explicitly designed to enhance both conductive and convective heat transfer mechanisms simultaneously. The SCR fin, with its combined flat conductive face and curved convective surface, represents such a geometry. However, no prior experimental study has systematically varied SCR fin spacing (δ) to optimize this balance, nor has one quantitatively evaluated its coupling with nanoparticle-enhanced PCM under controlled, high-flux conditions for PV cooling. This study addresses a critical gap: the lack of a systematic experimental investigation that parametrically studies SCR fin spacing and its synergistic coupling with nanoparticle-enhanced PCM for PV cooling. The SCR geometry inherently offers both an increased conductive surface area and a flat face that acts as a guide vane to organize natural convection. To the best of the authors' knowledge, such a focused parametric study has not been previously undertaken. This work presents a comprehensive experimental study into the combined influence of SCR fin geometry (with varied spacing ratio δ), fin pitch (λ), and alumina nanoparticle concentration (φ) on PV thermal regulation. A constant heat flux of 1000 W/m^2 is applied as a well-established methodological approach to provide a controlled, reproducible, and stringent benchmark for the fundamental comparison and ranking of different passive cooling configurations [29,61,65]. This method simulates a conservative, sustained peak thermal load, representing a worst-case scenario of continuous maximum solar irradiance, and allows for the clear isolation of each design's intrinsic thermal response and maximum heat dissipation capacity. Using a heated surface to simulate PV panels, system performance is evaluated in terms of temperature reduction and thermal buffering duration.

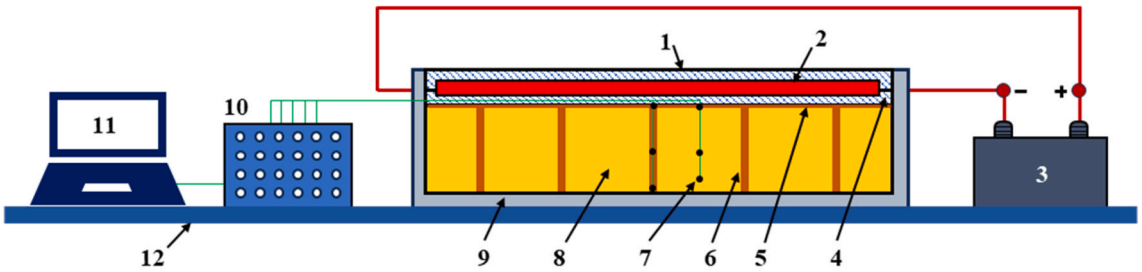

Fig. 1. Schematic representation of the experimental facility.

2. Experimental setup

The experimental setup is designed to evaluate the thermal performance of various passive PV cooling strategies under controlled laboratory conditions. Fig. 1 illustrates the complete facility. The experimental setup consists of a custom heater assembly that simulates PV heat generation, a copper sheet that serves as the simulated PV module's interface, an insulated PCM container, and integrated finned heat sinks. Two aluminum plates (200 × 200 × 4 mm) are separated by a precisely machined gap of 2.5 ± 0.1 mm. This gap accommodates a flat nickel-chrome wire heating element (2.4 Ω/m, total resistance 14.5 Ω). The heater is wound on a mica sheet (180 × 180 × 1 mm) and is encapsulated between two additional mica layers for electrical insulation and mechanical stability (Fig. 2a). The complete assembly is positioned between the aluminum plates (Fig. 2b). The heater connects to a regulated DC power supply. A digital multimeter is used to measure the input voltage and current to calculate the supplied electrical power accurately. This heater assembly is used to deliver a constant heat flux of 1000 ± 10 W/m^2 to a copper sheet, which represents the rear surface of a PV module. The ambient temperature is maintained at 28 ± 0.5 °C.

The application of a constant heat flux of 1000 W/m^2 for a duration of 3.5 h provides a controlled and reproducible benchmark for comparing passive cooling configurations. This methodological approach is widely adopted in experimental photovoltaic thermal management studies [29,60,65] and is also relevant for evaluating thermal regulation strategies in high-power electronic systems. The imposed steady-state condition represents a sustained peak thermal load, offering a conservative scenario that rigorously challenges the maximum heat dissipation capacity and intrinsic thermal response of each cooling design. While real-world solar irradiance is inherently transient and governed by diurnal and meteorological variations, the selected test duration corresponds to a concentrated period of high irradiance and approximates worst-case thermal operating conditions for photovoltaic modules. This enables focused evaluation of the system's ability to delay temperature rise and maintain effective thermal regulation under continuous high thermal loading. It is important to note that this approach simplifies the coupled electrical-thermal behavior of actual PV modules. In real installations, heat generation is linked to electrical output and varies with irradiance, temperature-dependent efficiency, and localized effects associated with cell interconnections. The constant heat flux surrogate does not capture these dynamic interactions. Accordingly, the thermal performance metrics reported in this study should be interpreted as comparative indicators of cooling effectiveness under sustained high thermal load, rather than as direct predictors of electrical efficiency enhancement under outdoor operating conditions. Future outdoor testing on functional PV modules is therefore recommended to validate the electrical performance implications of the proposed hybrid cooling strategy.

A cast acrylic container (200 × 200 × 30 mm) holds the PCM (RT35HC), with its thermophysical properties listed in Table 1. To enhance the PCM's effective thermal conductivity, γ-Al_2O_3 nanoparticles (properties in Table 2) are dispersed into the molten PCM at mass concentrations by weight (φ) of 0.25, 0.50, 0.75, and 1%. The preparation of nano-PCM mixtures involves mechanical stirring followed by ultrasonic agitation at 20 kHz for 2 h to ensure a homogeneous suspension. Verification of the melting temperature for both pure and nano-enhanced PCM occurs through repeated heating and cooling cycles in a water bath. The pure PCM exhibits a melting point of 35.18 °C, while the nano-PCM mixtures lead to a slight depression to 34.71, 33.52, 32.42, and 31.13 °C for φ = 0.25, 0.50, 0.75, and 1%, respectively. This depression is consistent with literature on nano-PCM and is attributed to the high surface area of nanoparticles that disrupts the PCM's crystal structure and nucleation dynamics [57,58]. A 25 mm thick fiberglass layer insulates the external walls of the acrylic container to minimize parasitic heat loss, ensuring the PCM system absorbs the vast majority of the input heat.

Copper fins are fabricated from solid copper rods (12.5 mm outer diameter, 30 mm height) to leverage copper's high thermal conductivity. The fin diameter is fixed at 12.5 mm based on a trade-off between enhanced conductive surface area, structural rigidity, and preservation of effective PCM volume. This dimension is sufficiently large to promote efficient heat spreading from the copper substrate while avoiding excessive blockage of buoyancy-driven flow within the molten PCM. In addition, the selected diameter facilitates precise fabrication and consistent soldering, ensuring good thermal contact and experimental repeatability. These fins are soldered to a thin 0.2 mm copper sheet, which is firmly fixed to the rear surface of the aluminum plate using thermally conductive silicone to minimize contact thermal resistance. The investigation covers two primary fin geometries: CCR and SCR, as shown in Fig. 3. The CCR fins are arranged in arrays,3 × 3, 4 × 4, and 5 × 5, corresponding to fin pitches (p_f) of 66.6, 50.0, and 40.0 mm, respectively. The SCR fins are used in a 5 × 5 array (p_f = 40.0 mm) but with varying base spacings (S) of 2, 4, and 6 mm between the flat surfaces of adjacent fins. The fin pitch and spacing are represented by the dimensionless ratios defined in Eqs. (1) and (2).

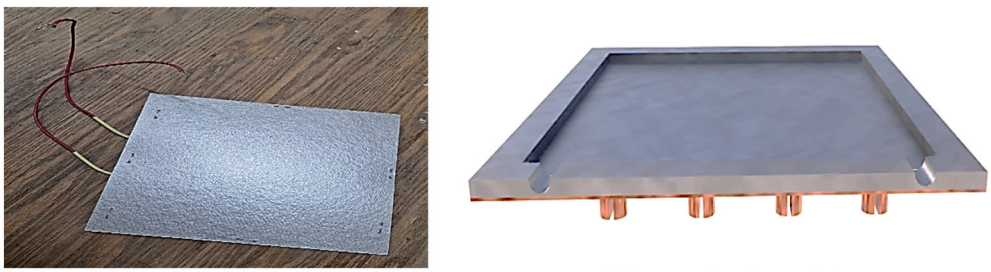

a) Electric heater b) Lower aluminum plate

Fig. 2. Representation of the heating element.

Table 1
Main characteristic specifications of the used PCM RT35HC.

Phase-change temperature (°C)	~34-36 °C (peak at 35 °C)	
Latent heat capacity (kJ/kg)	240 ± 7.5%	
Thermal conductivity (W/m·°C)	Solid:	0.334
	Liquid:	0.187
Density (kg/m^3)	Solid:	880
	Liquid:	770
Specific heat capacity (J/kg·°C)	Solid:	1570
	Liquid:	2000
Volume expansion	~12–15 % during melting	
Max operating temperature (°C)	70	

Table 2
Properties of γ-Al_2O_3 nanoparticles.

Primary particle size	~30 nm (20–50 nm range)
Density (kg/m^3)	3800
Specific surface area	>200 m^2/g
Purity	99.99%
Specific heat (at 25 °C)	880
Thermal conductivity (W/m·°C)	30
Appearance	Fine white nanopowder

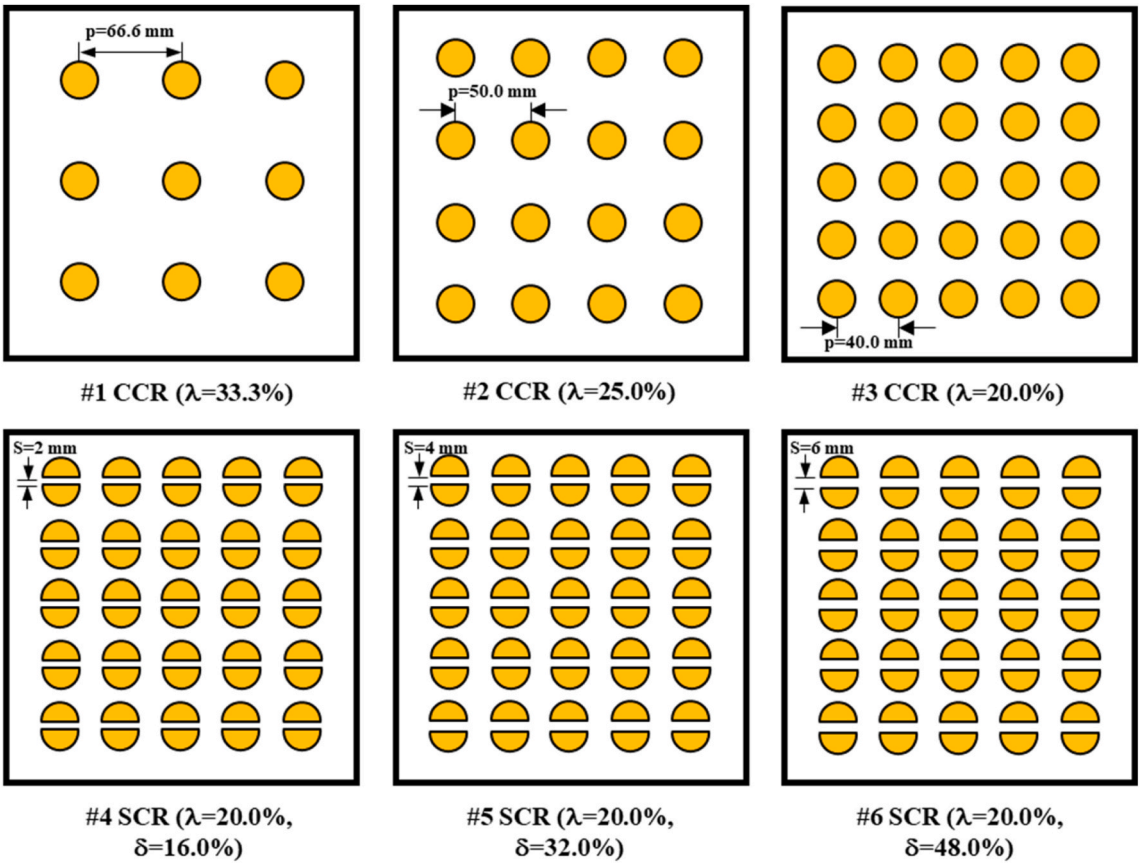

Fig. 3. Different configurations of the tested fins.

$$\lambda = \frac{p_f}{L_p} \tag{1}$$

$$\delta = \frac{S}{d_f} \tag{2}$$

The test matrix in detail is shown in Table 3, including twelve system configurations. These comprise a baseline (naturally cooled), a PCM-only case, three CCR fin cases, three SCR fin spacing configurations, and four cases with nanoparticle-enhanced PCM with the expected optimal SCR configuration. The nanoparticle mass concentration, φ, is calculated by:

$$\varphi = \frac{m_{np}}{m_{np} + m_{PCM}} \tag{3}$$

The temperatures are measured via twelve calibrated K-type thermocouples. Three thermocouples are fixed on the copper sheet at the interface (x/H = 0) to measure the simulated PV temperature. Another three thermocouples are attached onto the front surface of the upper aluminium plate. Two thermocouples are fixed on a selected fin: one at the mid-height (x/H = 0.5) and one at the tip near the container bottom (x/H = 1). The remaining four thermocouples are distributed within the PCM volume to capture the spatial temperature distribution and phase change progression: two at the mid-height (x/H = 0.50) and two near the container bottom (x/H = 0.85), as illustrated in Fig. 4. A multi-channel data acquisition system, connected to a personal computer, records all temperature data at a frequency of 1 Hz.

3. Experimental procedures and calculations

For each test, the PCM or nano-PCM is first melted, poured into the container, and allowed to solidify. The system is assembled, and the heater is activated only after thermal equilibrium with the ambient environment is reached. The power supply maintains a constant heat flux of 1000 W/m^2 for the entire 3.5-h experimental duration. Temperatures for analysis are reported as spatial averages: the copper sheet temperature (simulated PV module) is taken as the average of its three thermocouples, while the PCM temperatures at the mid-height (x/H = 0.50) and near the container bottom (x/H = 0.85) are taken as the average of their respective pairs of thermocouples. For each configuration, experiments are carried out three times to ensure repeatability and statistical reliability. The supplied electrical power (P_h) is calculated using the measured voltage (V) and current (I) as:

$$P_h = IV \tag{4}$$

The applied heat flux (q''_h) is then determined using Eq. (5), where A_h represents the effective heating area.

$$q''_h = \frac{P_h}{A_h} \tag{5}$$

The relative temperature reduction is quantified by the percentage reduction in the temperature rise above ambient, referenced to the uncooled baseline (Test #1), as:

$$\eta = \frac{T_{uncooled} - T_{cooled}}{T_{uncooled} - T_{ambient}} \tag{6}$$

4. Experimental uncertainty and statistical analysis

A comprehensive uncertainty analysis was performed to ensure the reliability and repeatability of the experimental measurements. The standard uncertainty associated with a single temperature measurement arises from thermocouple precision (±0.5 °C) and data acquisition error (±0.1 °C). Using the root-sum-square method [66], the resulting uncertainty for an individual temperature reading is ±0.51 °C. The uncertainty in spatially averaged temperatures is correspondingly reduced: for the copper sheet temperature, obtained

Table 3
Design parameters of the tested systems.

Test #	Cooling medium	Fins layout	No. of fins (N)	Fin pitch (p), mm	Pitch ratio (λ)	Base spacing, (S), mm	Spacing ratio (δ)	Mass concentration (φ)
1	No cooling (Insulated)							
2	PCM	-	-	-	-	-	-	0
3	PCM	CCR	9	66.6	33.3%	-	-	0
4			16	50.0	25.0%			
5			25	40.0	20.0%			
6	PCM	SCR	25	40.0	20%	2	16.0%	0
7						4	32.0%	
8						6	48.0%	
9	PCM + Al_2O_3	SCR	25	40.0	20%	6	48%	0.25%
10								0.50%
11								0.75%
12								1.00%

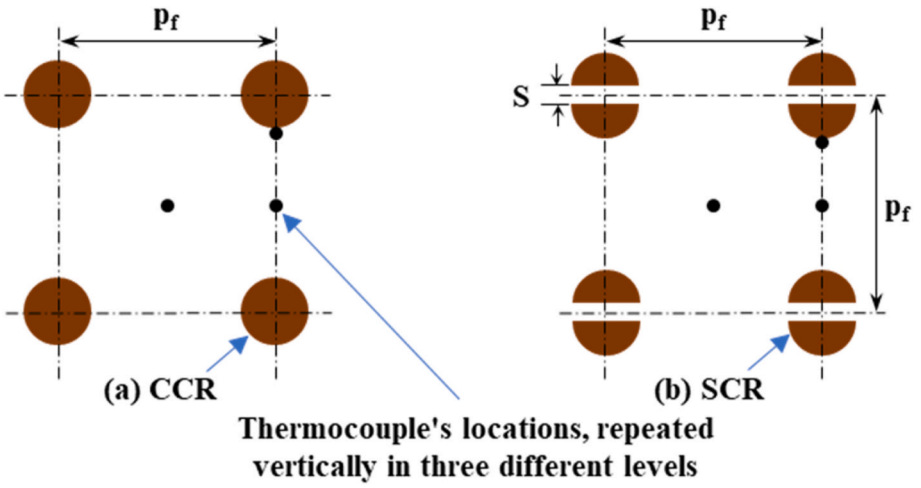

Fig. 4. Thermocouples locations in the tested system with (a) CCR and (b) SCR fins.

as the average of three measurements, the expanded uncertainty is ±0.29 °C, while for PCM temperatures at a given height, averaged from two measurements, the expanded uncertainty is ±0.36 °C. The uncertainties associated with voltage and current measurements are ±0.5% and ±1.0% of the reading, respectively. Applying standard uncertainty propagation using the same method [66], the maximum uncertainty in the calculated heat flux is estimated to be ±1.12%. The uncertainty in nanoparticle mass concentration is considered negligible due to the high precision of the analytical balance employed. Consequently, the maximum uncertainty in the reported relative temperature reduction (η) is estimated to be ±1.6%. A summary of the key experimental uncertainties discussed in this section is provided in Table 4 for ease of reference.

In addition to instrumental uncertainties, the potential influence of parasitic heat losses on the comparative results was evaluated. The test container was insulated using a 25 mm thick fiberglass layer with a thermal conductivity of approximately $k \approx 0.04 W/m.^{\circ}C$). Based on the exposed lateral wall area (≈0.024 m^2), insulation thickness, and a representative temperature difference of $\Delta T \approx 20$ °C between the PCM (≈48-51 °C) and the controlled ambient environment (28 °C), the estimated steady-state lateral heat loss is approximately 0.8 W. This corresponds to less than 2% of the total heat input imposed to the system (≈40 W, based on a heat flux of 1000 W/m^2 applied over a heated area of 0.04 m^2). Since the insulation, container geometry, and ambient conditions were identical for all tested configurations, this heat loss is systematic and comparable across experiments and therefore does not significantly affect the relative comparison of cooling performance metrics, including η, temperature reduction, and thermal buffering duration. The repeatability of the experiments is further supported by a consistently low standard deviation in the averaged copper sheet temperature, remaining within ±0.3 °C across all triplicate tests. This level of repeatability is consistent with the calculated uncertainty bounds and indicates a high degree of consistency in the observed experimental trends.

5. Validation of experimental setup

Before investigating enhanced cooling strategies, it is essential to validate the fundamental thermal response of the experimental apparatus itself. To this end, the uncooled baseline configuration (Test #1, Table 1) is compared against the results of Biwole et al. [29] for the baseline case under an identical heat flux of 1000 W/m^2. The comparative results are presented in Fig. 5. Despite differences in both orientation (present study: horizontal vs [29].: vertical) and ambient temperature (present: $T_{ambient,present} = 28^{\circ}C$ vs [29].: $T_{ambient,[31]} = 20^{\circ}C$), the thermal profiles exhibit strong agreement in both trend and magnitude. Both curves show a steep, quasi-linear temperature rise, characteristic of the baseline system under high heat flux. Over the 180-min test period, the average front-surface temperatures were $T_{ave,present} = 74.74^{\circ}C$ and $T_{ave,ref} = 69.63^{\circ}C$, respectively. To account for differences in ambient conditions, the average temperature rise above ambient is calculated for each case. The relative difference between these normalized temperature

Table 4
Summary of experimental measurement uncertainties.

Parameter	Expanded uncertainty
Single temperature measurement	±0.51 °C
Averaged copper sheet temperature	±0.29 °C
Averaged PCM temperature (per height)	±0.36 °C
Voltage measurement	±0.5%
Current measurement	±1.0%
Calculated heat flux	±1.12%
Relative temperature reduction (η)	±1.6%

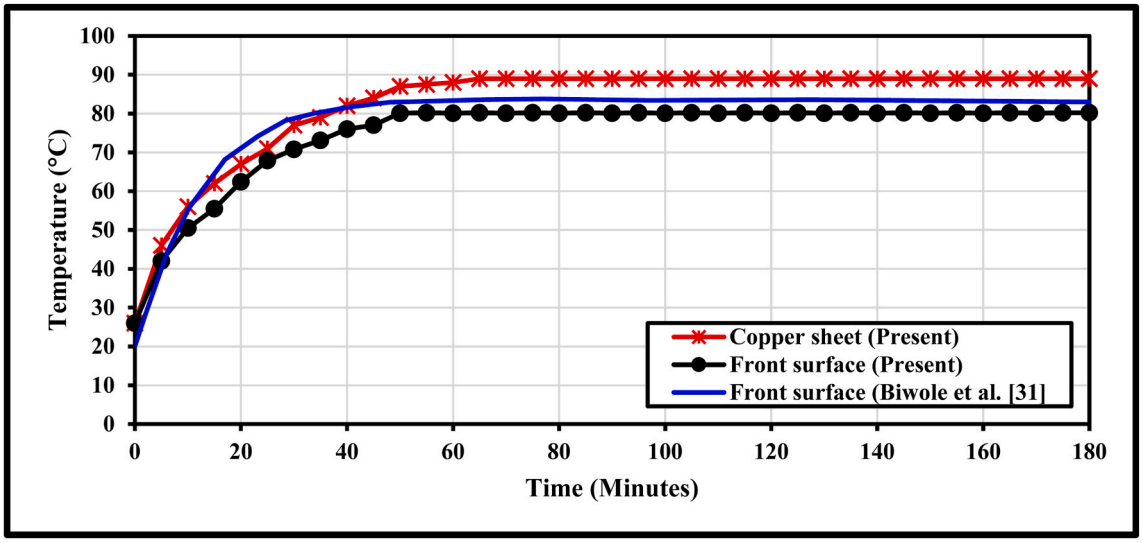

Fig. 5. Temperature profile of the baseline case #1 compared to the numerical data from Biwole et al. [29] under the same constant heat flux of 1000 W/m^2.

rises is:

$$\frac{\left|\Delta T_{ave,present} - \Delta T_{ave,ref}\right|}{\Delta T_{ave,ref}} * 100\% = \frac{|46.74 - 49.63|}{49.63} * 100\% \approx 5.8\% \quad (7)$$

This close quantitative agreement, achieved under more stringent ambient conditions, validates the fundamental thermal response of the experimental apparatus and establishes a reliable foundation for subsequent comparative analyses of enhanced cooling configurations.

6. Results and discussion

This section presents comprehensive experimental results and detailed analysis of various thermal management configurations for photovoltaic cooling applications. The investigation systematically evaluates the performance enhancement through multiple approaches: PCM integration, fin-assisted PCM systems, comparative analysis between different fin geometries, and nanoparticle enhancement techniques. Four primary aspects are thoroughly examined:

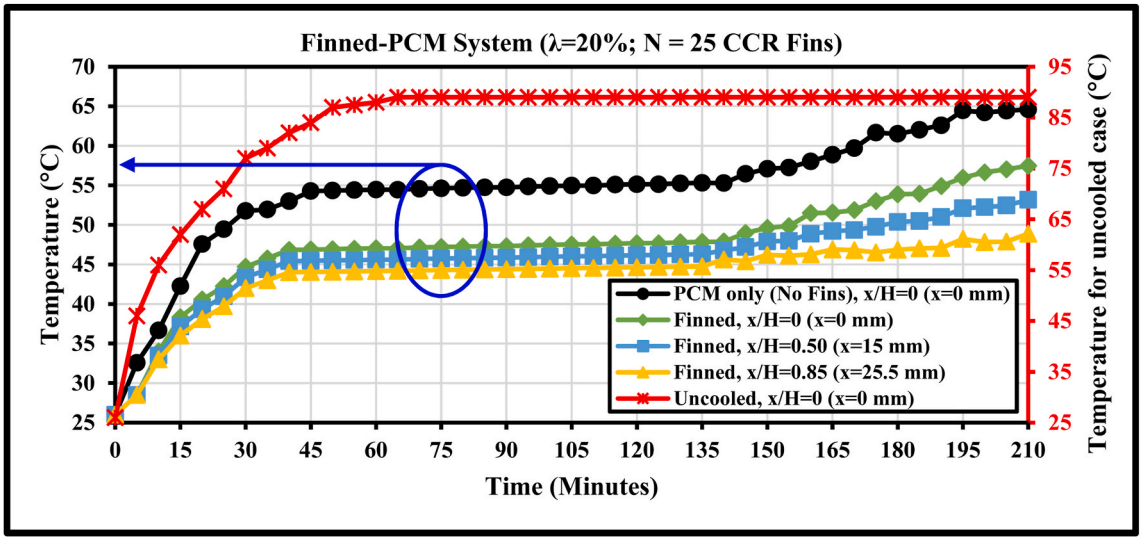

Fig. 6. Temperature profiles for baseline, PCM-only, and finned-PCM (CCR, λ = 20%) configurations.

- The fundamental benefits of integrating PCM with CCR fins, optimization of fin density through varying fin pitch ratios (λ),
- Performance comparison between CCR and SCR fin configurations with different spacing parameters (δ),
- Thermal performance improvement through the addition of alumina nanoparticles at various mass concentrations (φ).

All experiments maintain identical operating conditions with precise temperature monitoring at strategic locations within the PCM domain, ensuring reliable comparison and comprehensive assessment of thermal management strategies for photovoltaic systems.

6.1. *The effect of integrated PCM and CCR fins*

This section presents a detailed comparative analysis of three thermal management configurations for photovoltaic modules: the baseline system, a PCM-only system, and an integrated finned-PCM system employing 25 CCR fins with $\lambda = 20\%$. The investigation systematically evaluates thermal performance using temperature measurements from the copper sheet interface, which serves as the simulated PV module, supplemented by data from thermocouples distributed within the PCM domain, and along with a representative fin to provide comprehensive insight into heat transfer characteristics. The experimental results, comprehensively detailed in Fig. 6, demonstrate measurable and progressive improvements in thermal performance with each system enhancement, highlighting the critical importance of integrated cooling solutions for photovoltaic applications. The baseline reference configuration exhibits rapid thermal saturation, with the copper sheet reaching ~89.0 °C within 65 min and achieving an asymptotic temperature throughout the 210-min test duration. This performance profile illustrates the severe thermal challenge facing conventional PV modules, characterized by an extremely steep initial temperature gradient that climbs from 26 °C to 46 °C in just 5 min and reaches 67 °C within 20 min, demonstrating virtually no thermal buffering capacity.

In contrast, the PCM-only configuration provides a noticeable improvement, with the copper sheet temperature limited to 61.4 °C after 210 min, corresponding to a relative temperature reduction of $\eta = 45.2\%$ compared to the baseline case. The temperature rise is more gradual; the system requires 35 min to reach 51.5 °C, whereas the baseline system reaches a higher temperature of 62 °C within 15 min. However, the thermal response reveals a key limitation. Between 10 and 20 min, during the primary phase change interval of the RT35HC PCM, the temperature increases sharply from 35.9 °C to 45.6 °C. The absence of a pronounced isothermal plateau and the nearly 10 °C rise over this 10-min interval indicate that the inherently low thermal conductivity of the PCM constrains heat diffusion into the bulk material. Under the applied heat flux of 1000 W/m^2, this leads to localized melting near the heat source and a transition to dominant sensible heating, thereby preventing full utilization of the PCM's latent heat capacity. These observations underscore the need for an effective thermal conductivity enhancement mechanism.

The integrated finned-PCM configuration exhibits further improvement in thermal regulation, with the copper sheet temperature reaching only 54.6 °C after 210 min, corresponding to $\eta = 56.1\%$ relative to the baseline system and a clear enhancement compared to the PCM-only case. In addition, the finned system demonstrates a substantially improved thermal buffering capability. While the baseline configuration exceeds the critical temperature threshold of 47.0 °C within approximately 10 min, and the PCM-only system within about 23 min, the finned-PCM system maintains temperatures below this threshold for approximately 145 min. Similarly, operation below 50 °C is sustained for about 185 min. Rather than indicating a fundamental change in operating behavior, these results demonstrate a significant extension of the safe operating window under sustained peak thermal loading. This improvement is directly attributed to the CCR fins acting as effective thermal bridges between the heat source and the PCM bulk. Temperature measurements within the PCM domain reveal a stable spatial gradient at t = 210 min, decreasing from 54.6 °C at the copper interface (x/H = 0) to

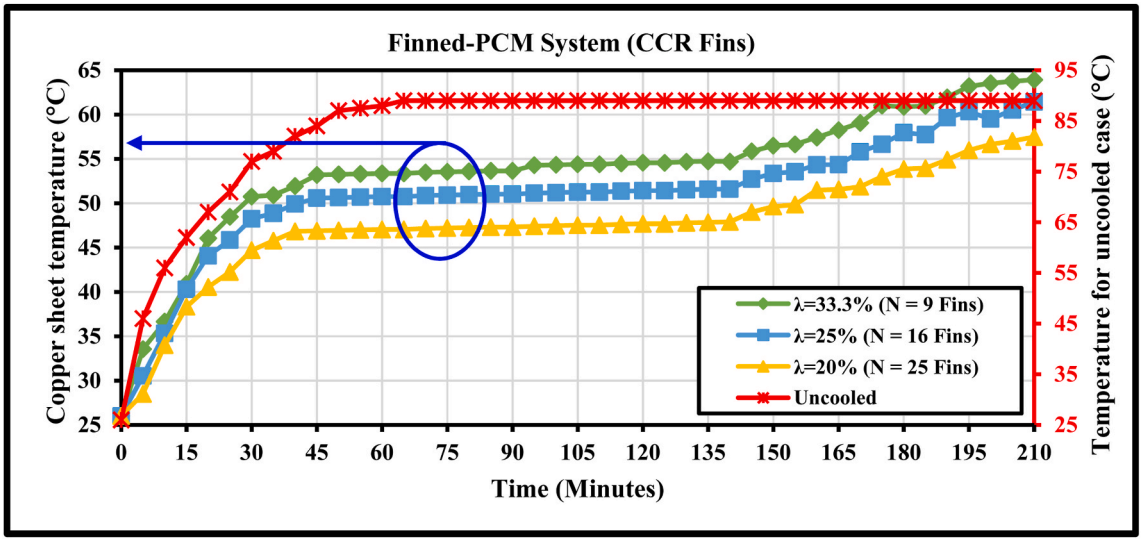

Fig. 7. Temperature profiles for CCR fin systems with different pitch ratios (λ).

50.5 °C at mid-height (x/H = 0.50), and further to 46.4 °C near the container bottom (x/H = 0.85), corresponding to a total gradient of 8.2 °C. This sustained gradient confirms enhanced conductive heat transport into the PCM bulk, a mechanism that is largely absent in the PCM-only configuration and directly addresses its primary thermal limitation.

The overall thermal regulation results from the combined contributions of sensible heat storage, latent heat absorption, and fin-enhanced conduction. During the initial heating period, sensible storage in the PCM and metallic components is dominant. As the interface temperature reaches the PCM melting point, latent absorption becomes the primary energy-storage mechanism, extending the near-isothermal operational window. The fins do not store significant energy themselves but critically reduce the thermal resistance between the heat source and the PCM, thereby accelerating the rate at which energy is delivered to the PCM volume and enabling more uniform and effective utilization of its latent-heat capacity. After complete melting, sensible heating again governs the final temperature rise. A detailed time-resolved energy partition would require complementary calorimetric measurements or numerical simulation, which represent a valuable direction for further fundamental analysis.

6.2. *The effect of the number of fins*

The present investigation also examines how fin density, characterized by the dimensionless pitch ratio λ, influences the thermal performance of finned-PCM systems for photovoltaic cooling applications. Distinct CCR fin configurations, with three different pitch ratios of λ = 33.3% (9 fins), λ = 25% (16 fins), and λ = 20% (25 fins), are evaluated under identical experimental conditions, with temperature measurements consistently recorded at the copper sheet interface (x/H = 0). The experimental results are presented in Fig. 7. The results demonstrate a clear correlation between increasing fin density and enhancement in the cooling performance, with progressively lower final temperatures achieved as fin count increases. The 9-fin configuration reaches a final temperature of 60.3 °C (η = 47.0%), while the 16-fin and 25-fin systems achieve 57.9 °C (η = 51.0%) and 54.6 °C (η = 56.1%), respectively, establishing a 6.5 °C overall improvement from the lowest to highest fin density configuration.

Analysis of the transient thermal response highlights distinct performance regimes across the tested fin densities. During the initial 50 min, all configurations exhibit comparable behavior, with temperature differences remaining within 2.0 °C. Beyond this period, the thermal responses diverge significantly. The 9-fin configuration shows a continuous temperature rise throughout the remaining test duration, whereas the 25-fin system maintains temperatures below the critical threshold of 47.0 °C for approximately 150 min, followed by a more gradual increase. The 16-fin configuration exhibits intermediate behavior, sustaining sub-47 °C temperatures for approximately 145 min. These trends reflect the role of fin density in improving heat transfer mechanisms, where additional fins provide multiple parallel conductive pathways that reduce thermal resistance between the heat source and the PCM, enabling more uniform heat distribution.

The substantial increase in effective heat transfer surface area, approximately 178% for the 25-fin configuration compared to the 9-fin case, quantitatively explains the observed 5.7 °C difference in final temperature. The denser fin arrangement also promotes faster heat penetration into the PCM bulk, allowing a larger PCM volume to participate in latent heat absorption. Temporal analysis further indicates that the 25-fin configuration delays the temperature rise to 50.0 °C by approximately 110 min relative to the 9-fin system, while extending the operating duration below 50 °C from 75 to 135 min, representing an 80% increase in effective thermal buffering time. Such performance improvements are particularly relevant for photovoltaic applications, where sustained operation at lower temperatures during peak solar loading is critical for maintaining efficiency and reliability. It should be noted, however, that while increasing fin density enhances conductive heat spreading and accelerates PCM engagement within the investigated range, further

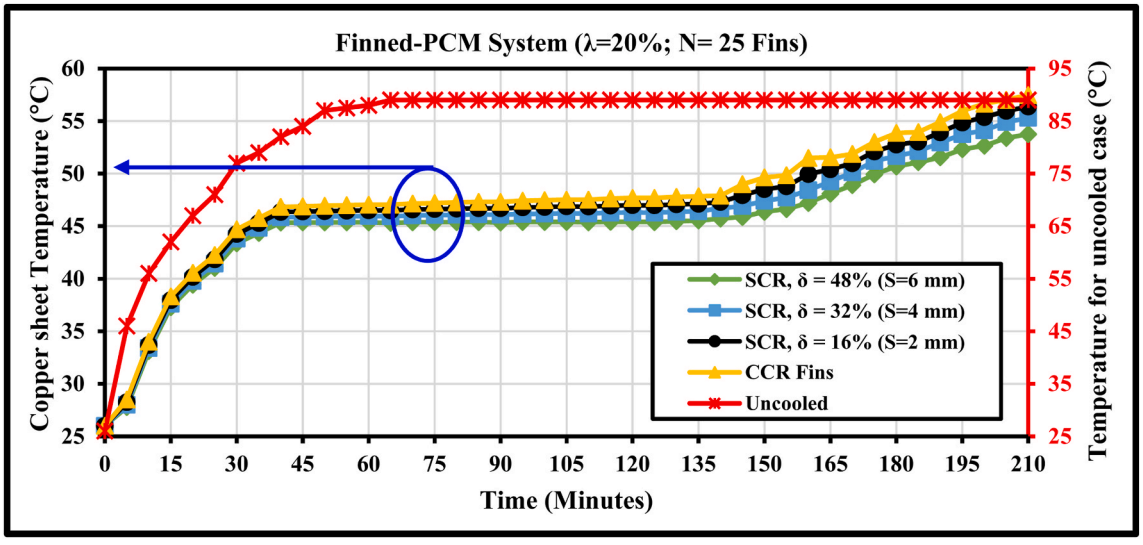

Fig. 8. Temperature profiles for CCR and SCR fin configurations.

increases beyond λ = 20% are expected to result in diminishing thermal returns. Excessive fin density may reduce the effective PCM volume, restrict buoyancy-driven convection within the molten PCM, and introduce additional manufacturing complexity. Accordingly, the λ = 20% configuration represents a practical upper bound within the present experimental scope, offering a balanced compromise between thermal performance enhancement and system simplicity.

6.3. Comparison between CCR and SCR fin configurations

In the present work, the thermal performance differences between Complete Circular Rod (CCR) and Semicircular Rod (SCR) fin configurations are investigated through systematic experimental analysis. The study evaluates the previously established optimal CCR configuration (λ = 20%, N = 25 fins) against three distinct SCR configurations with varying spacing ratios δ (δ = S/D, where S represents the normal distance between SCR fin bases and D denotes the fin diameter). The SCR configurations maintain identical fin count while employing spacing ratios of δ = 16% (S = 2 mm), δ = 32% (S = 4 mm), and δ = 48% (S = 6 mm) to thoroughly assess spacing effects on thermal performance. The experimental results presented in Fig. 8 show that SCR configurations achieve improved thermal performance compared to the conventional CCR design throughout the entire 210-min test period. The optimal SCR system (δ = 48%) reaches a final temperature of 51.0 °C. This represents a substantial η = 62.3%, meaning it prevented nearly two-thirds of the temperature rise seen in the uncooled case. This represents a measurable improvement over the CCR configuration. The 3.6 °C temperature reduction provided by the optimal SCR configuration relative to the CCR design can potentially contribute to improved conversion efficiency and long-term reliability in photovoltaic systems.

The enhanced thermal performance of SCR fins originates from fundamental improvements in both conductive and convective heat transfer mechanisms. Geometrically, while a single CCR fin provides a cylindrical surface area of $A_{CCR} = \pi DH$, the same spatial footprint can accommodate two back-to-back SCR fins. Each SCR fin contributes a semicylindrical outer surface and a flat rectangular face. Therefore, the combined heat-dissipating surface area for the SCR pair is:

$$A_{SCR} = \pi DH + 2DH \tag{8}$$

Compared to the area of one CCR fin (πDH), this represents a relative increase of:

$$\frac{A_{SCR} - A_{CCR}}{A_{CCR}} = \frac{\pi DH + 2DH - \pi DH}{\pi DH} = \frac{2}{\pi} = 0.6366 = 63.66\% \tag{9}$$

This significant increase in the area available for heat exchange with the PCM enhances conductive heat transfer. More importantly, the sharp edges of the flat surface effectively disrupt thermal boundary layers, while the flat face itself acts as a guide vane that organizes and strengthens natural convection currents within the PCM. This promotes more efficient mixing of the molten PCM and accelerates the heat dissipation process through enhanced fluid dynamics. From a fluid-dynamic perspective, the flat face of the SCR fin modifies buoyancy-driven convection compared to the cylindrical CCR geometry. The planar heated surface promotes more coherent upward plume formation similar to natural convection over a vertical plate, whereas cylindrical fins tend to generate more circumferential and distributed plume detachment. The sharp transition edges of the SCR geometry may also contribute to local boundary layer thinning and earlier boundary layer disruption, enhancing the local heat transfer coefficient. Furthermore, the flat surface acts as a guiding interface that organizes inter-fin recirculation structures and reduces stagnant zones near the fin base, thereby improving melt uniformity and bulk mixing within the molten PCM. Although these mechanisms were not directly visualized in the present study, they are consistent with the observed improvement in system-level thermal performance.

Moreover, from a dimensionless heat transfer perspective, the superior performance of the SCR geometry can be interpreted in terms of its influence on buoyancy-driven convection within the molten PCM. The semicircular profile modifies the internal flow domain and characteristic length scale governing natural convection between adjacent fins, thereby affecting the effective Rayleigh number and the development of thermal boundary layers. The increased conductive surface area of the SCR fins further enhances heat spreading, which in turn influences the overall Nusselt number by coupling conductive and convective mechanisms. While the present study provides clear system-level evidence of improved thermal performance, direct quantification of Rayleigh and Nusselt numbers would require spatial temperature mapping, flow visualization, or numerical simulations to resolve local velocity and thermal fields. Accordingly, the derivation of a generalized dimensionless heat transfer correlation for SCR configurations lies beyond the scope of this experimental investigation and represents a valuable direction for future fundamental analysis. The clear performance hierarchy among SCR configurations reveals the critical importance of geometric optimization. The system with the largest spacing (δ = 48%) demonstrates optimal performance, while intermediate spacing (δ = 32%) and smallest spacing (δ = 16%) configurations attain final temperatures of 52.5 °C and 53.5 °C, respectively. The progressive 2.5 °C temperature reduction with increasing inter-fin spacing indicates that the benefit of increased surface area must be balanced with sufficient clearance to allow unimpeded development of natural convection currents within the PCM. The optimal spacing (δ = 48%) provides this balance by maximizing both conductive area and convective flow to facilitate the most efficient utilization of the PCM's latent heat capacity.

Detailed examination of the temperature progression data confirms that SCR configurations consistently maintain lower temperatures than the CCR system throughout the experimental duration. During the critical first 140-min period, the optimal SCR system maintains temperatures approximately 1.5-2.0 °C lower than the CCR configuration. This early-stage thermal advantage proves particularly valuable for practical applications where rapid thermal response during initial operation is essential for maintaining optimal performance. The thermal performance data clearly shows that the SCR configuration with δ = 48% maintains temperatures below 45 °C for 150 min compared to 45 min for the CCR configuration, providing a 233% longer duration at this optimal operating temperature. The comprehensive experimental evidence establishes that SCR configurations, particularly with optimized spacing

ratios, provide superior thermal management compared to traditional CCR designs. The significant temperature reduction achieved through the SCR fin geometry results directly from the combined effects of increased heat transfer surface area and enhanced PCM convection coefficient enabled by the unique semicircular rod geometry. This represents an effective approach for thermal management applications that directly translates to improved system efficiency and enhanced operational reliability, positioning SCR configurations as the preferred choice for high-efficiency cooling systems where maximum performance and reliability are essential requirements.

6.4. The effect of alumina nanoparticles on thermal performance

The integration of alumina nanoparticles within the phase change material, combined with the optimized semicircular rod fin configuration, yields measurable improvements in thermal performance through multiple enhancement mechanisms. Experimental evaluation for four nanoparticle mass concentrations (0.25-1.0 wt%) reveals a distinct concentration-dependent improvement trend, with systematic enhancement observed across all measured parameters. A summary of key performance metrics for nano-PCM systems is presented in detail in Table 5. Fig. 9 shows the temperature progression data confirm consistent performance improvement with increasing nanoparticle loading, establishing a clear correlation between nanoparticle concentration and cooling efficacy.

The system incorporating 1.0% nanoparticles achieves optimal performance, reaching a final temperature of 48.8 °C. This corresponds to $\eta = 65.9\%$, an improvement over the 62.3% relative temperature reduction of the pure PCM system with SCR fins. The improved thermal response of the nano-PCM system can be interpreted in the context of classical effective medium theory. For the 1.0 wt% Al_2O_3 nano-PCM employed in this study, the corresponding nanoparticle volume fraction is approximately ≈0.2%. Application of the Maxwell model [67] for spherical particles predicts an intrinsic thermal conductivity enhancement of only ~0.5%. This modest increase indicates that the experimentally observed system-level performance gains cannot be attributed solely to a significant rise in thermal conductivity. Instead, the enhancement is more plausibly associated with a synergistic combination of modest conductive improvement, nanoparticle-induced melting point depression, and potential alterations in nucleation behavior and buoyancy-driven convection during melting. These findings highlight the multifaceted role of nanoparticles in improving PCM thermal performance beyond simple conductivity enhancement.

The augmented thermal transport properties facilitate more efficient heat dissipation from the copper substrate through the fin network into the PCM bulk, reducing thermal resistance and promoting accelerated heat distribution with more uniform phase change progression. Material characterization reveals nanoparticle-induced melting point depression from 35.18 °C for pure PCM to 31.13 °C for the 1.0% nanocomposite, attributed to disrupted crystal structure and altered nucleation dynamics caused by the high-surface-area nanoparticles. This shift in the phase change temperature range means that the latent heat absorption begins at a lower system temperature, providing proactive thermal buffering earlier in the heating cycle. Analysis of the thermal profiles demonstrates notably improved thermal regulation capabilities during the critical initial heating period, where the 1.0% nano-PCM system maintains temperatures 1.2-1.5 °C lower than the pure PCM system throughout the first 140 min of the experiment operation. The comprehensive performance metrics confirm that the nano-enhanced system extends the operational duration below 45 °C by 15 min, representing a 12.5% extension of optimal operating conditions compared to the pure PCM system. These thermal improvements suggest potential electrical efficiency benefits for photovoltaic applications. Based on the established temperature coefficient for crystalline silicon solar cells (−0.4% to −0.5% per 1 °C), the measured cooling corresponds to a projected relative electrical efficiency improvement of 16.1-20.1% compared to the uncooled baseline. This projection is derived from the thermal performance data using the well-documented thermal-electrical relationship of PV cells, highlighting the indicative electrical benefit inferred from temperature reduction. However, this projection does not account for real operating conditions such as irradiance variability, electrical loading, and coupled electro-thermal effects, and should therefore be interpreted as an indicative estimate rather than a directly measured performance gain.

The long-term reliability of the optimal hybrid configuration, comprising SCR fins ($\delta = 48\%$, $\lambda = 20\%$) and a 1.0 wt% Al_2O_3 nano-PCM composite, was assessed over 300 accelerated thermal cycles. This approach is consistent with prior nano-PCM studies that use thermal cycling as a proxy for colloidal stability in the absence of direct rheological characterization [68,69]. Fig. 10 presents the evolution of the interface temperature and relative temperature reduction as a function of cycle count, indicating stable system performance throughout the testing period. The endpoint temperature increased by only 0.3 °C, from 48.8 °C to 49.1 °C, while the relative temperature reduction decreased by just 0.5% points over the entire testing regimen. This limited variation corresponds to an average performance change of approximately 0.0017% per cycle, indicating stable system-level thermal performance under repeated phase change operation. The stability is further reflected in the highly repeatable thermal response observed during successive melting and solidification cycles, indicating consistent system-level heat transfer behavior. Although no direct physicochemical characterization of nanoparticle sedimentation or agglomeration was conducted, the minimal performance drift suggests that any nanoparticle

Table 5
Summary of key performance metrics for nano-PCM systems.

Nanoparticle Concentration	Final Temperature (°C)	Relative temperature reduction, η (%)	Time Below 45 °C (min)
0% (Pure PCM)	51.0	62.3	150
0.25%	50.3	63.4	175
0.50%	49.5	64.8	179
0.75%	49.2	65.2	181
1.00%	48.8	65.9	185

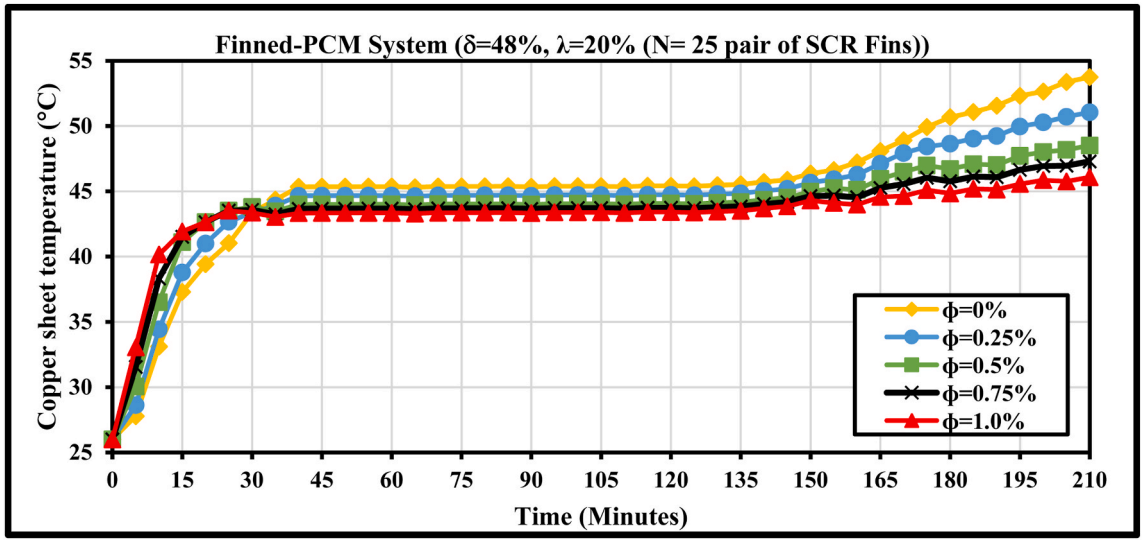

Fig. 9. Temperature profiles for SCR fin systems with different nanoparticle concentrations (φ).

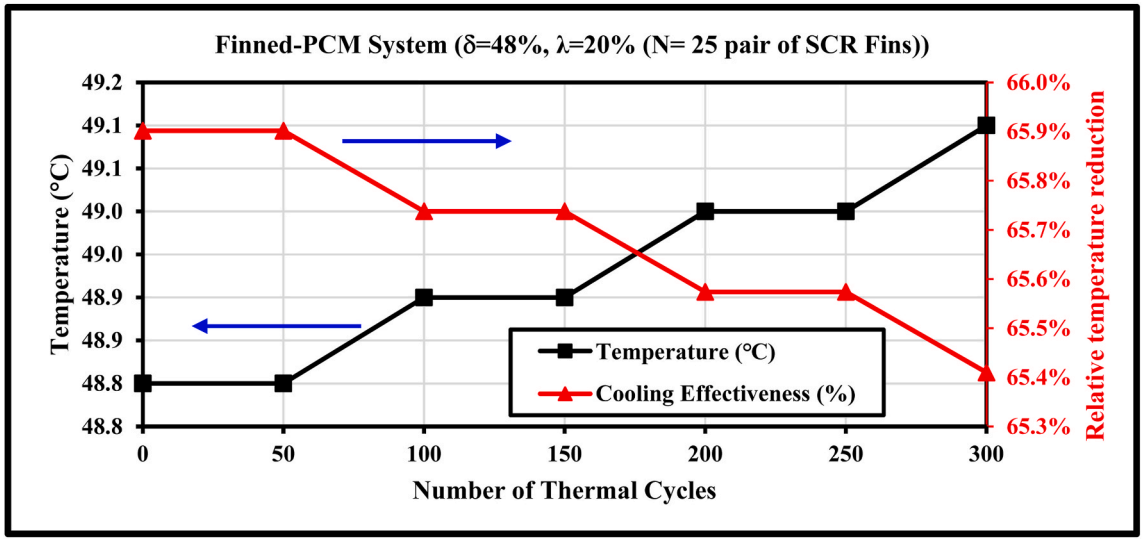

Fig. 10. Temperature and relative temperature reduction (η) over 300 thermal cycles for the optimal hybrid system.

redistribution during cycling did not adversely affect the overall thermal response within the experimental timeframe. Nevertheless, extended outdoor exposure, long-term aging, and environmental factors such as vibration and thermal stratification may influence nanoparticle dispersion over service lifetimes, and therefore warrant further investigation under real operating conditions.

In addition to the accelerated thermal cycling results, it is important to consider potential degradation mechanisms that may influence long-term performance under multi-year operation. For the present system, the primary projected mechanisms include copper fin surface oxidation, nanoparticle agglomeration or sedimentation within the PCM matrix, PCM leakage during repeated phase transitions, and possible interfacial thermal resistance evolution between the copper fins, PCM, and container walls. Copper oxidation could gradually increase interfacial thermal resistance; however, under the enclosed and insulated conditions of the present system, such effects are expected to progress slowly and mainly become relevant under prolonged outdoor exposure. Nanoparticle agglomeration or redistribution may alter local thermal transport properties over long durations, particularly under sustained thermal gradients, although the minimal performance drift observed over 300 accelerated cycles suggests that any such effects are limited within the investigated timeframe. PCM leakage and interfacial delamination were not observed during testing, indicating adequate mechanical and thermal compatibility of the selected materials. Nevertheless, extended outdoor exposure, long-term aging, vibration, and environmental effects may influence these mechanisms over service lifetimes. Accordingly, the present durability assessment should be interpreted as a demonstration of short-to medium-term stability, while long-term field testing remains necessary to fully quantify

multi-year reliability under realistic operating conditions.

6.5. Comparative analysis with previous studies

The experimental results presented in the preceding sections indicate effective thermal regulation of the hybrid SCR fin and nano-PCM cooling strategy. To contextualize these findings within the existing literature, a comparative analysis of representative PV-PCM and nano-PCM cooling studies is presented in this section. Owing to substantial differences among published works, including heat flux levels, PCM type and mass, fin geometry, boundary conditions, module orientation, and evaluation metrics, the comparison is intentionally qualitative in nature rather than a direct quantitative benchmark. Table 6 summarizes selected studies to highlight relative performance trends and dominant enhancement mechanisms. While absolute temperature reduction (ΔT) is reported for reference, it should be interpreted as an indicative metric rather than a strict basis for one-to-one comparison. The objective of this analysis is to extract general design insights rather than to claim numerical equivalence across studies.

Within this qualitative framework, the present results consistently indicate that geometric enhancement plays a dominant role in improving PCM-based passive cooling performance. Multiple finless nano-PCM systems reported in the literature exhibit limited temperature reduction despite high nanoparticle loadings, suggesting that enhanced thermal conductivity alone is insufficient to overcome heat spreading limitations. In contrast, finned configurations generally demonstrate improved thermal regulation by facilitating heat distribution and promoting buoyancy-driven convection within the PCM. The SCR fin configuration investigated in this study represents an advanced geometric approach that combines increased conductive surface area with guided natural convection pathways. Compared to conventional ribs or cylindrical fins reported in earlier studies, the SCR geometry provides improved thermal coupling between the heat source and the PCM bulk. When combined with modest nanoparticle loading, this geometric optimization yields a synergistic enhancement effect that extends thermal buffering duration and reduces peak operating temperatures. Although some active PV/T systems report cooling improvements under specific operating conditions, their performance is inherently influenced by auxiliary energy input and increased system complexity. The present comparison therefore highlights the potential of well-designed fully passive systems to achieve competitive thermal regulation without operational energy consumption. Overall, the qualitative comparison reinforces the central conclusion of this work that co-optimization of fin geometry and PCM properties is more impactful than material enhancement alone in passive thermal management applications.

7. Conclusions

The present comprehensive experimental investigation demonstrates the effectiveness of a hybrid passive cooling strategy for regulating temperature in systems subjected to high heat flux. The key findings and their implications are as follows:

- The integration of fins is found to be critical for unlocking PCM performance. The optimal CCR fin system ($\lambda = 20\%$) achieved a final temperature of 54.6 °C, corresponding to $\eta =$ of 56.1%. More significantly, it extended the operational period below 50 °C from just 12 min for the uncooled baseline to 185 min, demonstrating a significant improvement in thermal buffering.
- Fin geometry is a decisive factor for the PV system performance. The optimal SCR configuration ($\delta = 48\%$, $\lambda = 20\%$) achieved a final temperature of 51.0 °C, $\eta = 62.3\%$ and a 3.6 °C improvement over the best CCR design, demonstrating the advantage of the SCR geometry.
- Nanoparticles provide a significant, concentration-dependent enhancement. The highest concentration ($\varphi = 1.0\%$) yielded the best performance, reaching a final temperature of 48.8 °C, which corresponds to $\eta = 65.9\%$.
- A hierarchical optimization strategy delivers the highest performance. The optimal hybrid system (1.0% nano-PCM with SCR fins, $\delta = 48\%$, $\lambda = 20\%$) combines the enhanced conduction of nanoparticles with the superior heat spreading capability of an optimized fin geometry, achieving a total temperature reduction of 40.2 °C from the uncooled baseline.

While the experimental context simulated a PV module, the results also suggest promising potential for the thermal management of high-power electronic components. The ability to maintain a simulated surface temperature below 50 °C under a constant heat flux of 1000 W/m^2 for an extended period demonstrates a viable solution for managing heat in similar compact electronic systems. The passive nature of this system offers key advantages for electronics, including inherent reliability, zero power draw for cooling, and silent operation. This work demonstrates that the hybrid SCR fin/nano-PCM strategy offers an effective passive thermal management approach from a thermal perspective, achieving a temperature reduction of 40.2 °C under a sustained heat flux of 1000 W/m^2. The substantial cooling achieved indicates significant potential for improving photovoltaic electrical performance, as indirectly estimated using standard PV temperature coefficients, subject to validation through direct electrical measurements under realistic operating conditions. The approach also shows considerable promise for thermal management in high-power electronic systems.

Future work will focus on: (i) outdoor testing of the hybrid system on operational PV modules to quantify actual electrical efficiency gains, (ii) direct electrical performance measurements under realistic irradiance profiles (iii) long-term material-stability studies (e.g., nanoparticle sedimentation, PCM-fin interfacial durability), over extended thermal cycling, and (iv) numerical simulations or flow-visualization experiments to resolve local velocity and temperature fields, enabling the development of a dimensionless heat-transfer correlation for SCR-fin PCM systems. These steps will further validate the practical viability and durability of this passive cooling approach and provide deeper fundamental insight into its convective enhancement mechanisms.

Table 6
Qualitative comparison of representative PCM-based passive and hybrid cooling strategies reported in the literature.

Study/System Type	Nanoparticle/PCM	Loading (φ)	System Configuration	$\Delta T_{reduction}$ (°C)	Key Finding & Distinction of Present Work
Present Study Experimental; Passive	Al_2O_3/RT35HC	1.0 wt%	Novel SCR Fins (δ = 48%, λ = 20%)	40.2 (from 89 to 48.8 °C)	Demonstrates the combined influence of optimized fin geometry and moderate nano-PCM loading on enhancing passive thermal regulation.
Zhou et al. [70] Experimental; Passive	Boron Nitride/ Paraffin Wax	10 wt%	No Fins (Composite only)	21.4 (from 59 to 37.6 °C)	Illustrates the limitations of finless nano-PCM systems despite high nanoparticle loading.
Soliman [30] Experimental; Passive	PCM	–	Ribs	19.8 (from 82 to 62.2 °C)	Shows the role of basic geometric enhancement in improving PCM heat dissipation.
Jamil et al. [71] Experimental; Passive	Graphene/PT58	0.5 wt%	No Fins	10 (from 66.4 to 56.4 °C)	Indicates modest thermal improvement from nanoparticles without geometric heat spreading.
Jamil et al. [72] Experimental; Passive	CB/PT58	0.5 wt%	No Fins	9.8 (from 68 to 58.2 °C)	Suggests similar performance trends among different nanoparticles in finless configurations.
Sheik et al. [73] Experimental; Passive	Al_2O_3/PEG-1000	20 wt%	No Fins	9 (from 52.4 to 43.4 °C)	Highlights diminishing returns of high nanoparticle loading without geometric enhancement.
Jamil et al. [72] Experimental; Passive	SiO_2/PT-58	0.5 wt%	No Fins	8.1 (from 68 to 59.9 °C)	Reinforces the dominant limitation imposed by the absence of fins.
Sheik et al. [73] Experimental; Passive	SiO_2/PEG-1000	20 wt%	No Fins	7.8 (from 52.7 to 44.9 °C)	Demonstrates performance ceiling in finless PCM systems regardless of nanoparticle type.
Kibria et al. [74] Experimental; Active PV/T	Al_2O_3/ZnO (Hybrid)/Paraffin Wax	2 wt%	No Fins (with water cooling)	5.4 (from 61.5 to 56.1 °C)	Represents active cooling performance influenced by auxiliary energy input and system complexity.
Karunesh et al. [75] Numerical; Passive	CuO/RT35	5 wt%	No Fins	1.7 (from 78.4 to 76.7 °C)	Numerically predicts limited impact of nanoparticles without geometric heat spreading.

CRediT authorship contribution statement

Menna M. Hamed: Writing – original draft, Validation, Methodology, Investigation, Formal analysis, Data curation. **Mohamed R. Salem:** Writing – review & editing, Validation, Supervision, Resources, Project administration, Methodology, Investigation, Formal analysis, Data curation, Conceptualization. **Abdulmajeed D. Aldabesh:** Writing – review & editing, Validation, Resources, Methodology, Formal analysis. **Sayed A. Abdel-Moneim:** Writing – review & editing, Validation, Supervision, Methodology, Investigation, Formal analysis, Conceptualization. **Ashraf E. Elmohlawy:** Writing – review & editing, Validation, Supervision, Resources, Investigation, Formal analysis, Data curation.

Declaration of competing interest

We confirm that there are not any financial and personal relationships with other people or organizations that could inappropriately influence our work. In addition, we confirm that this work is original and has not been published elsewhere nor is it currently under consideration for publication elsewhere.

Data availability

Data will be made available on request.

References

[1] F. Odoi-Yorke, R. Opoku, F. Davis, G. Obeng, Optimisation of thermal energy storage systems incorporated with phase change materials for sustainable energy supply: a systematic review, Energy Rep. 10 (2023) 2496–2512, https://doi.org/10.1016/j.egyr.2023.09.044.
[2] M. Ghamari, C. See, D. Hughes, T. Mallick, K. Reddy, K. Patchigolla, S. Sundaram, Advancing sustainable building through passive cooling with phase change materials, a comprehensive literature review, Energy Build. 312 (2024) 114164, https://doi.org/10.1016/j.enbuild.2024.114164.
[3] M. Amir, R. Deshmukh, H. Khalid, Z. Said, A. Raza, S.M. Muyeen, A. Nizami, R. Elavarasan, R. Saidur, K. Sopian, Energy storage technologies: an integrated survey of developments, global economical/environmental effects, optimal scheduling model, and sustainable adaption policies, J. Energy Storage 72 (Part E) (2023) 108694, https://doi.org/10.1016/j.est.2023.108694.
[4] M. Worku, Recent advances in energy storage systems for renewable source grid integration: a comprehensive review, Sustainability 14 (10) (2022) 5985, https://doi.org/10.3390/su14105985.
[5] G. Merabet, M. Essaaidi, M. Haddou, B. Qolomany, J. Qadir, M. Anan, A. Al-Fuqaha, M. Abid, D. Benhaddou, Intelligent building control systems for thermal comfort and energy-efficiency: a systematic review of artificial intelligence-assisted techniques, Renew. Sustain. Energy Rev. 144 (2021) 110969, https://doi.org/10.1016/j.rser.2021.110969.

[6] A. Behzadi, S. Holmberg, C. Duwig, F. Haghighat, R. Ooka, S. Sadrizadeh, Smart design and control of thermal energy storage in low-temperature heating and high-temperature cooling systems: a comprehensive review, Renew. Sustain. Energy Rev. 166 (2022) 112625, https://doi.org/10.1016/j.rser.2022.112625.
[7] S. Rashidi, N. Karimi, B. Sunden, K. Kim, A. Olabi, O. Mahian, Progress and challenges on the thermal management of electrochemical energy conversion and storage technologies: fuel cells, electrolysers, and supercapacitors, Prog. Energy Combust. Sci. 88 (2022) 100966, https://doi.org/10.1016/j.pecs.2021.100966.
[8] M. Salem, R. Ali, K. Elshazly, Experimental investigation of the performance of a hybrid photovoltaic/thermal solar system using aluminium cooling plate with straight and helical channels, Sol. Energy 157 (2017) 147–156, https://doi.org/10.1016/j.solener.2017.08.019.
[9] D. Cabaleiro, F. Agresti, L. Fedele, S. Barison, C. Hermida-Merino, S. Losada-Barreiro, S. Bobbo, M. Piñeiro, Review on phase change material emulsions for advanced thermal management: design, characterization and thermal performance, Renew. Sustain. Energy Rev. 159 (2022) 112238, https://doi.org/10.1016/j.rser.2022.112238.
[10] Z. Qin, C. Ji, Z. Low, W. Tong, C. Wu, F. Duan, Geometry effect of phase change material container on waste heat recovery enhancement, Appl. Energy 327 (2022) 120108, https://doi.org/10.1016/j.apenergy.2022.120108.
[11] M. Moreira, T. Silva, J. Dias-de-Oliveira, F. Neto, C. Amaral, Numerical modelling of radiant systems and phase change materials in building applications - a review, Appl. Therm. Eng. 234 (2023) 121342, https://doi.org/10.1016/j.applthermaleng.2023.121342.
[12] Z. Li, G. Fu, L. Fan, Synergistic effects of nano-enhanced phase change material (NePCM) and fin shape on heat storage performance of a finned shell-and-tube unit: an experimental study, J. Energy Storage 45 (2022) 103772, https://doi.org/10.1016/j.est.2021.103772.
[13] A. Karthick, M. Athikesavan, M. Pasupathi, N. Kumar, S. Chopra, A. Ghosh, Investigation of inorganic phase change material for a semi-transparent photovoltaic (STPV) module, Energies 13 (14) (2020) 3582, https://doi.org/10.3390/en13143582.
[14] C. Podara, I. Kartsonakis, C. Charitidis, Towards phase change materials for thermal energy storage: classification, improvements and applications in the building sector, Appl. Sci. 11 (2021) 1490, https://doi.org/10.3390/app11041490.
[15] U. Masood, M. Haggag, A. Hassan, M. Laghari, A review of phase change materials as a heat storage medium for cooling applications in the built environment, Buildings 13 (7) (2023) 1595, https://doi.org/10.3390/buildings13071595, 1595.
[16] T. Ma, J. Zhao, J. Han, A parametric study about the potential to integrate phase change material into photovoltaic panel, Energy Proc. 142 (2017) 648–654, https://doi.org/10.1016/j.egypro.2017.12.107.
[17] P. Kumar, G. Mukesh, S. Naresh, D. Mohana Nitthilan, R. Kumar, Study on Performance Enhancement of SPV Panel Incorporating a Nanocomposite PCM as Thermal Regulator, Materials, Design, and Manufacturing for Sustainable Environment, Springer Singapore, 2021, pp. 587–597, https://doi.org/10.1007/978-981-15-9809-8_44.
[18] M. Huang, P. Eames, B. Norton, Thermal regulation of building-integrated photovoltaics using phase change materials, Int. J. Heat Mass Tran. 47 (12–13) (2004) 2715–2733, https://doi.org/10.1016/j.ijheatmasstransfer.2003.11.015.
[19] F. Díaz, N. Moraga, R. Cabrales, Computational modeling of a PV-PCM passive cooling system during a day-night cycle at arid and semi-arid climate zones, Energy Convers. Manag. 270 (2022) 116202, https://doi.org/10.1016/j.enconman.2022.116202.
[20] A. Shafai, E. Hadi, S. Taher, M. Salem, A. Elmohlawy, Numerical analysis of enhancing latent heat storage using fins and conductive barriers, J. Al-Azhar Univ. Eng. Sector 20 (75) (2025) 450–465, https://doi.org/10.21608/auej.2025.332683.1727.
[21] G. Simonsen, R. Ravotti, P. O'Neill, A. Stamatiou, Biobased phase change materials in energy storage and thermal management technologies, Renew. Sustain. Energy Rev. 184 (2023) 113546, https://doi.org/10.1016/j.rser.2023.113546.
[22] M. Rinawa, S. Selvasofia, P. Kumar, R. Subbiah, R. Saminathan, M. Singh, P. Saravanakumar, G. Brain, V. Eswarlal, Analyzing an evacuated tube solar water heating system using twin-nano/paraffin as phase change material, Mater. Today Proc. 50 (Part 5) (2022) 2505–2509, https://doi.org/10.1016/j.matpr.2021.10.500.
[23] P. Saravanakumar, S. Arunkumar, B. Mansingh, P. Kumar, R. Subbiah, V. Eswarlal, Investigating the effect of thermal cycling on thermal characteristics of the nano-silica based phase changing material (PCM), Mater. Today Proc. 50 (Part 5) (2022) 1502–1507, https://doi.org/10.1016/j.matpr.2021.09.095.
[24] S. Bhakre, P. Sawarkar, V. Kalamkar, Experimental study on photovoltaic panel integrated with polyethylene glycol 1500 phase change material, J. Energy Storage 55 (Part B) (2022) 105518, https://doi.org/10.1016/j.est.2022.105518.
[25] Z. Said, F. Ahmad, A. Radwan, A. Hachicha, New thermal management technique for PV module using Mist/PCM/Husk: an experimental study, J. Clean. Prod. 401 (2022) 136798, https://doi.org/10.1016/j.jclepro.2023.136798.
[26] E. Amalu, O. Fabunmi, Thermal control of crystalline silicon photovoltaic (c-Si PV) module using Docosane phase change material (PCM) for improved performance, Sol. Energy 234 (2022) 203–221, https://doi.org/10.1016/j.solener.2022.02.001.
[27] M. Maghrabie, A. Mohamed, A. Fahmy, A. Abdel Samee, Performance enhancement of PV panels using phase change material (PCM): an experimental implementation, Case Stud. Therm. Eng. 42 (2023) 102741, https://doi.org/10.1016/j.csite.2023.102741.
[28] K. Prakash, M. Pasupathi, S. Chinnasamy, S. Saravanakumar, M. Palaniappan, A. Alasiri, M. Chandrasekaran, Energy and exergy enhancement study on PV systems with phase change material, Sustainability 15 (4) (2023) 3627, https://doi.org/10.3390/su15043627.
[29] P. Biwole, P. Eclache, F. Kuznik, Phase-change materials to improve solar panel's performance, Energy Build. 62 (2013) 59–67, https://doi.org/10.1016/j.enbuild.2013.02.059.
[30] A. Soliman, 4E analysis of a new design heat sink for cooling a bifacial photovoltaic system using PCM and ribs, J. Energy Storage 73 (2023) 108907, https://doi.org/10.1016/j.est.2023.108907.
[31] J. Kim, H. Naganathan, S. Moon, D. Jang, Optimizing comfort and sustainability: the impact of passive cooling and eco-friendly materials on indoor temperature reduction-a case study, Buildings 14 (10) (2024) 3218, https://doi.org/10.3390/buildings14103218.
[32] B. Debich, A. El Hami, A. Yaich, W. Gafsi, L. Walha, M. Haddar, Design optimization of PCM-based finned heat sinks for mechatronic components: a numerical investigation and parametric study, J. Energy Storage 32 (2020) 101960, https://doi.org/10.1016/j.est.2020.101960.
[33] I. Zahid, M. Farooq, M. Farhan, M. Usman, A. Qamar, M. Imran, M. Alqahtani, S. Anwar, M. Sultan, M. Javaid, Thermal performance analysis of various heat sinks based on alumina NePCM for passive cooling of electronic components: an experimental study, Energies 15 (22) (2022) 8416, https://doi.org/10.3390/en15228416.
[34] K. Shah, P. Ong, M. Chua, S. Toh, J. Lee, X. Soo, Z. Png, R. Ji, J. Xu, Q. Zhu, Application of phase change materials in building components and the use of nanotechnology for its improvement, Energy Build. 262 (2022) 112018, https://doi.org/10.1016/j.enbuild.2022.112018.
[35] Z. Maqbool, M. Hanief, M. Parveez, Review on performance enhancement of phase change material based heat sinks in conjugation with thermal conductivity enhancers for electronic cooling, J. Energy Storage 60 (2023) 106591, https://doi.org/10.1016/j.est.2022.106591.
[36] X. Zheng, Y. Zhou, A three-dimensional unsteady numerical model on a novel aerogel-based PV/T-PCM system with dynamic heat-transfer mechanism and solar energy harvesting analysis, Appl. Energy 338 (2023) 120899, https://doi.org/10.1016/j.apenergy.2023.120899.
[37] B. Emmanuel, Y. Yuan, B. Maxime, N. Gaudence, J. Zhou, A review on the influence of the components on the performance of PVT modules, Sol. Energy 226 (2021) 365–388, https://doi.org/10.1016/j.solener.2021.08.042.
[38] S. Abdul-Ganiyu, D. Quansah, E. Ramde, R. Seidu, M. Adaramola, Study effect of flow rate on flat-plate water-based photovoltaic-thermal (PVT) system performance by analytical technique, J. Clean. Prod. 321 (2021), https://doi.org/10.1016/j.jclepro.2021.128985.
[39] H. Joo, Y. An, M. Kim, M. Kong, Long-term performance evaluation of liquid-based photovoltaic thermal (PVT) modules with overheating-prevention technique, Energy Convers. Manag. 296 (2023) 117682, https://doi.org/10.1016/j.enconman.2023.117682.
[40] N. Alipour, B. Jafari, K. Hosseinzadeh, Analysis of the impact of metal foam with phase change material on solar photovoltaic thermal system efficiency, J. Energy Storage 98 (Part A) (2024) 113064, https://doi.org/10.1016/j.est.2024.113064.
[41] K. Parach, B. Jafari, K. Hosseinzadeh, Numerical analysis of integrated photovoltaic thermal systems utilizing nanoparticles with phase change material and fin attachments, Int. J. Thermofluids 27 (2025) 101210, https://doi.org/10.1016/j.ijft.2025.101210.
[42] S. Nada, M. Said, Effects of fins geometries, arrangements, dimensions and numbers on natural convection heat transfer characteristics in finned-horizontal annulus, Int. J. Therm. Sci. 137 (2018) 121–137, https://doi.org/10.1016/j.ijthermalsci.2018.11.026.

[43] Y. Lee, Y. Liao, L. Chien, F. Cheung, A. Yang, Performance enhancement of latent heat thermal energy storage systems via dynamic melting process of PCM under different control strategies, Appl. Therm. Eng. 259 (2025) 124903, https://doi.org/10.1016/j.applthermaleng.2024.124903.
[44] Y. Huang, X. Liu, Charging and discharging enhancement of a vertical latent heat storage unit by fractal tree-shaped fins, Renew. Energy 174 (2021) 199–217, https://doi.org/10.1016/j.renene.2021.04.066.
[45] K. Hosseinzadeh, M. Moghaddam, A. Asadi, A. Mogharrebi, B. Jafari, M. Hasani, D. Ganji, Effect of two different fins (longitudinal-tree like) and hybrid nano-particles (MoS_2-TiO_2) on solidification process in triplex latent heat thermal energy storage system, Alex. Eng. J. 60 (1) (2021) 1967–1979, https://doi.org/10.1016/j.aej.2020.12.001.
[46] R. Oliveski, F. Becker, L. Rocha, C. Biserni, G. Eberhardt, Design of fin structures for phase change material (PCM) melting process in rectangular cavities, J. Energy Storage 35 (2021) 102337, https://doi.org/10.1016/j.est.2021.102337.
[47] A. Bria, B. Raillani, D. Chaatouf, M. Salhi, S. Amraqui, A. Mezrhab, Effect of PCM thickness on the performance of the finned PV/PCM system, Mater. Today Proc. 72 (Part 7) (2023) 3617–3625, https://doi.org/10.1016/j.matpr.2022.08.409.
[48] M. Masoumpour-Samakoush, M. Miansari, S. Ajarostaghi, M. Arıcı, Impact of innovative fin combination of triangular and rectangular fins on melting process of phase change material in a cavity, J. Energy Storage 45 (2022) 103545, https://doi.org/10.1016/j.est.2021.103545.
[49] Q. Li, J. Jiang, Y. Hong, J. Du, Numerical investigation of thermal management performances in a solar photovoltaic system by using the phase change material coupled with bifurcated fractal fins, J. Energy Storage 56 (Part C) (2022) 106156, https://doi.org/10.1016/j.est.2022.106156.
[50] J. Jiang, Y. Hong, Q. Li, J. Du, Numerical analysis on heat transfer and melting characteristics of a solid-liquid phase change process in a rectangular cavity inserted with bifurcated fractal fins, Int. Commun. Heat Mass Tran. 142 (2023) 106616, https://doi.org/10.1016/j.icheatmasstransfer.2023.106616.
[51] J. Jiang, Y. Hong, Q. Li, J. Du, Evaluating the impacts of fin structures and fin counts on photovoltaic panels integrated with phase change material, Energy 283 (2023) 129143, https://doi.org/10.1016/j.energy.2023.129143.
[52] A. Chibani, S. Merouani, H. Laidoudi, A. Dehane, M. Morakchi, L. Bendada, Analysis and optimization of concentrator photovoltaic system using a phase change material (RT 35HC) combined with variable metal fins, J. Energy Storage 72 (Part B) (2023) 108283, https://doi.org/10.1016/j.est.2023.108283.
[53] C. Zhang, N. Wang, H. Xu, Y. Fang, Q. Yang, F. Talkhoncheh, Thermal management optimization of the photovoltaic cell by the phase change material combined with metal fins, Energy 263 (2023) 125669, https://doi.org/10.1016/j.energy.2022.125669.
[54] A. Mohammadpour, B. Jafari, K. Hosseinzadeh, Thermal enhancement analysis of PCM-filled finned tube heat exchangers using metal foams in building HVAC systems, J. Build. Eng. 120 (2026) 115276, https://doi.org/10.1016/j.jobe.2026.115276.
[55] H. Senobar, M. Aramesh, B. Shabani, Nanoparticles and metal foams for heat transfer enhancement of phase change materials: a comparative experimental study, J. Energy Storage 32 (2020) 101911, https://doi.org/10.1016/j.est.2020.101911.
[56] M. Hayat, Y. Chen, A Brief Review on Nano Phase Change Material-based Polymer Encapsulation for Thermal Energy Storage Systems, Energy and Sustainable Futures: Springer Proceedings in Energy, Springer, Cham, 2021, pp. 19–26, https://doi.org/10.1007/978-3-030-63916-7_3.
[57] Z. Said, A. Pandey, A. Tiwari, B. Kalidasan, F. Jamil, A. Thakur, V. Tyagi, A. Sarı, H. Ali, Nano-enhanced phase change materials: fundamentals and applications, Prog. Energy Combust. Sci. 104 (2024) 101162, https://doi.org/10.1016/j.pecs.2024.101162.
[58] M. Salem, M. Elsayed, A. Abd-Elaziz, K. Elshazly, Performance enhancement of the photovoltaic cells using Al2O3/PCM mixture and/or water cooling-techniques, Renew. Energy 138 (2019) 876–890, https://doi.org/10.1016/j.renene.2019.02.032.
[59] M. Moein-Jahromi, H. Rahmanian-Koushkaki, S. Rahmanian, S. Jahromi, Evaluation of nanostructured GNP and CuO compositions in PCM-based heat sinks for photovoltaic systems, J. Energy Storage 53 (2022) 105240, https://doi.org/10.1016/j.est.2022.105240.
[60] H. Abdelrahman, M. Wahba, H. Refaey, M. Moawad, N. Berbish, Performance enhancement of photovoltaic cells by changing configuration and using PCM (RT35HC) with nanoparticles Al_2O_3, Sol. Energy 177 (2019) 665–671, https://doi.org/10.1016/j.solener.2018.11.022.
[61] I. Zarma, M. Ahmed, S. Ookawara, Enhancing the performance of concentrator photovoltaic systems using Nanoparticle-phase change material heat sinks, Energy Convers. Manag. 179 (2019) 229–242, https://doi.org/10.1016/j.enconman.2018.10.055.
[62] A. Abdelrazik, F. Al-Sulaiman, R. Saidur, Numerical investigation of the effects of the nano-enhanced phase change materials on the thermal and electrical performance of hybrid PV/thermal systems, Energy Convers. Manag. 205 (2020) 112449, https://doi.org/10.1016/j.enconman.2019.112449.
[63] A. Najafpour, E. Montazer, K. Hosseinzadeh, A. Ranjbar, D. Ganji, J. Kanesan, Computational study on the impact of geometric parameters on the overall efficiency of multi-branch channel heat sink in the solar collector, Int. Commun. Heat Mass Tran. 158 (2024) 107884, https://doi.org/10.1016/j.icheatmasstransfer.2024.107884.
[64] W. Lin, Z. Ma, S. Wang, M. Sohel, E. Cascio, Experimental investigation and two-level model-based optimisation of a solar photovoltaic thermal collector coupled with phase change material thermal energy storage, Appl. Therm. Eng. 182 (2021) 116098, https://doi.org/10.1016/j.applthermaleng.2020.116098.
[65] M. Huang, P. Eames, B. Norton, Phase change materials for limiting temperature rise in building integrated photovoltaics, Sol. Energy 80 (2006) 1121–1130, https://doi.org/10.1016/j.solener.2005.10.006.
[66] S. Kline, F. McClintock, Describing uncertainties in single-sample experiments, Mech. Eng. 75 (1) (1953) 3–8.
[67] J.C. Maxwell, Treatise on Electricity and Magnetism, first ed., Clarendon Press, Oxford, UK, 1873.
[68] K. Kumar, K. Balasubramanian, B. Jinshah, N. Abhishek, Experimental analysis and neural network model of MWCNTs enhanced phase change materials, Int. J. Thermophys. 43 (2022) 11, https://doi.org/10.1007/s10765-021-02937-3.
[69] X. Guo, K. Zheng, H. Shi, L. Chen, Y. Shen, J. Chen, X. Tao, M. Yu, Thermal regulation of photovoltaic panels using shape-stabilized phase change materials supported by exfoliated graphite/graphene nanofillers, J. Clean. Prod. 446 (2024) 141435, https://doi.org/10.1016/j.jclepro.2024.141435.
[70] W. Zhou, Y. Wei, D. Wan, Experimental study and optimization the performance of photovoltaic panels using composite of phase change materials and boron nitride nanoparticles, J. Energy Storage 112 (2025) 115526, https://doi.org/10.1016/j.est.2025.115526.
[71] F. Jamil, H. Ali, M. Nasir, M. Karahan, M. Janjua, A. Naseer, A. Ejaz, R. Pasha, Evaluation of photovoltaic panels using different nano phase change material and a concise comparison: an experimental study, Renew. Energy 169 (2021) 1265–1279, https://doi.org/10.1016/j.renene.2021.01.089.
[72] F. Jamil, M. Khiadani, H. Ali, M. Nasir, S. Shoeibi, Thermal regulation of photovoltaics using various nano-enhanced phase change materials: an experimental study, J. Clean. Prod. 414 (2023) 137663, https://doi.org/10.1016/j.jclepro.2023.137663.
[73] M. Sheik, M. Aravindan, N. Beemkumar, P. Chaurasiya, R. Jilte, S. Shaik, A. Afzal, Investigation on the thermal management of solar photo voltaic cells cooled by phase change material, J. Energy Storage 52 (Part B) (2022) 104914, https://doi.org/10.1016/j.est.2022.104914.
[74] M. Kibria, M. Mohtasim, U. Paul, B. Das, R. Saidur, Impact of hybrid nano PCM (paraffin wax with Al_2O_3 and ZnO nanoparticles) on photovoltaic thermal system: energy, exergy, exergoeconomic and enviroeconomic analysis, J. Clean. Prod. 436 (2024) 140577, https://doi.org/10.1016/j.jclepro.2024.140577.
[75] K. Kant, A. Anand, A. Shukla, A. Sharma, Heat transfer study of building integrated photovoltaic (BIPV) with nano-enhanced phase change materials, J. Energy Storage 30 (2020) 101563, https://doi.org/10.1016/j.est.2020.101563.

Nomenclatures

A: Area, m^2
D: Fin diameter, m
H: Total PCM thickness (Fin height), m
I: Electrical current, A
L: Length, m
N: Number of fins
P: Electrical power, W
p: Fin pitch, m
q'': Heat flux, W/m^2

S: Base spacing, m
T: Temperature, °*C*
t: Time, s
V: Voltage drop, V
x: Distance from copper sheet, m

Greek Letters

φ: Nanoparticles' mass concentration
Δ: Differential
η: Relative temperature reduction
γ: Gamma; the type of used alumina nanoparticles
λ: Fin pitch ratio
δ: Fin spacing ratio

Sub Scripts

ave: Average
f: Fin
h: Heater
np: Nanoparticles
p: Plate
ref: Reference

Acronyms and Abbreviations

CCR: Complete Circular Rod
CPU: Central Processing Unit
PCM: Phase change material
PV: Photovoltaic
PV/T: Photovoltaic/Thermal
SCR: Semicircular Rod